analytical chemistry

Article

pubs.acs.org/ac

Dielectric Cell Response in Highly Conductive Buffers

Fabrice Gielen,[†,‡] Andrew J. deMello,[†,‡,§] and Joshua B. Edel*[,†,‡]

[†]Department of Chemistry and [‡]Institute of Chemical Biology, Imperial College London, South Kensington, London, SW7 2AZ, United Kingdom

[§]Department of Chemistry and Applied Biosciences, ETH Zurich, HCI F 117, Wolfgang-Pauli-Strasse 10, CH-8093 Zurich, Switzerland

Supporting Information

ABSTRACT: We present a novel method for the identification of live and dead T-cells, dynamically flowing within highly conductive buffers. This technique discriminates between live and dead (heat treated) cells on the basis of dielectric properties variations. The key advantage of this technique lies in its operational simplicity, since cells do not have to be resuspended in isotonic low conductivity media. Herein, we demonstrate that at 40 MHz, we are able to statistically distinguish between live and dead cell populations.

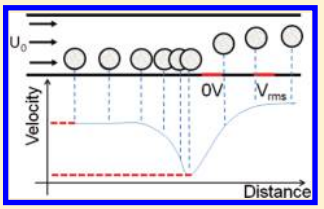

Downloaded via ETH ZURICH on February 21, 2019 at 13:41:09 (UTC).
See https://pubs.acs.org/sharingguidelines for options on how to legitimately share published articles.

The use of dielectrophoretic (DEP) forces as a tool to discriminate cell populations based on dielectric properties has triggered much interest over the last few decades.[1−3] For example, physical separation of cells or bacteria can be readily achieved by utilizing the differences between the polarizability of cells and suspending media. Such differences have been addressed theoretically and quantified as a function of membrane conductivity, capacitance, thickness, cell cytoplasm conductivity, permittivity, and cell radius.[4] These parameters have been integrated into the effective single-shell model, which can be used to accurately predict mammalian cell behavior in applications such as cellular trapping, discrimination, and separation.[5]

Historically, the most sensitive and practical dielectric identification schemes are those relying on cells immersed in an isotonic low conductivity medium.[6−8] This is due to the DEP response of cells or bacteria switching between a negative DEP regime (where cells are less polarizable than the buffer) and a positive DEP regime (where cells are more polarizable than the buffer) in low conductivity media. Such an effect introduces an observable change in behavior which can be quantified in terms of the crossover frequency (where the cell's response to the electric field is zero). However, this transition is highly frequency dependent and dictates a complex analysis of the response. In contrast, cells suspended in high conductivity buffers always undergo negative DEP (cells always remain less polarizable than the buffer regardless of operating frequency).

One key challenge when using a low conductivity medium is to reduce its impact on cell long-term viability.[9] By keeping cells in physiological buffers (of high conductivity), the cell environment is left unmodified throughout the analysis process. This ensures cell viability and increases the potential throughput of the overall identification procedure. The key disadvantage of using a high conductivity medium lies in the possibility of sample heating and electrochemical damage. However, these effects can be minimized by using low actuation voltages and applying high frequencies.[10]

Techniques extracting dielectric parameters such as electrorotation making use of phase shifts in multielectrode architectures or cell levitation experiments can derive the magnitude of the dielectric response for a wide frequency range based on the rotation rate of cells or levitation height, respectively.[11,12] Unfortunately, most of these configurations lack the ability to screen a large number of cells as the cells are not flowing continuously but rather staying in the detection zone. An alternative method is field flow fractionation DEP (DEP-FFF), which separates particles under nDEP based on their elution time in a Poiseuille flow configuration over interdigitated electrodes.[13] However, this technique can only operate at low throughput since cells have to be injected simultaneously at the start of the analysis chamber and acquisition times are long.

In the current work, we extend the latter concept by developing an identification tool, able to monitor changes in cellular response under nDEP in a high conductivity medium. In this situation, cells can be continuously floated over the detection zone with analytical throughput being limited by the flow rate of the cells which is limited by the global polarization response time and the cell density. Specifically, we show that high-frequency responses of live and dead cells cause differences in the flow pattern over the identification zone. The temporal and spatial interaction between cells and electrodes is maximized by leveraging geometrical and electrical confinement effects within a shallow polydimethysiloxane (PDMS) microchannel (30 μm deep).

EXPERIMENTAL METHODS

Jurkat T-cells were cultured in a 37 °C incubator with 5% CO_2 inside a growing solution of RPMI + 10% FBS + 1% L-glutamine and resuspended in 1X Dulbecco's phosphate

Received: August 22, 2011
Accepted: December 10, 2011
Published: December 10, 2011

 © 2011 American Chemical Society

buffered saline (Ca^{2+}/Mg^{2+}-free). The buffer composition was 2.6 mM KCl, 1.4 mM KH_2PO_4, 136 mM NaCl, and 8.1 mM Na_2HPO_4 (Sigma Aldrich). Cells were equally split in two aliquots. One aliquot was heated for 20 min at 65 °C, mixed with the other aliquot and 20% Trypan Blue solution (Sigma). The overall mixture conductivity was measured to be 1.35 S/m. Jurkat cells were measured by image analysis of miscroscopy pictures. The live cells had an average diameter of 10.2 ± 3.5 μm, and the dead cells had an average diameter of 10.7 ± 3.5 μm.

Microfluidic chips were fabricated as described previously, using Cr/Au parallel electrodes (15 μm wide with a 15 μm gap) deposited on a thin glass coverslip and covered by a 1 mm wide, 5 mm long, and 30 μm deep PDMS microchannel.[14] A function generator (4086-ND, Digikey Corporation) was used to provide electrical excitation at a voltage of 5 Vpp and at a frequency of either 1 MHz or 40 MHz.

Flow was initiated by a precision syringe pump (PHD 2000, Harvard Apparatus) using an air-free 1 mL Becton-Dickinson syringe connected to PTFE tubing of internal diameter 200 μm. Liquid was infused across the whole width of the microchannel. Cellular trajectories were monitored using a CCD camera (Phantom, v5.1, Vision Research) at a frame rate of 50 fps and at a resolution of 1024 × 512 pixels taken through a 40× objective of an Olympus IX71 microscope.

DEVICE OPERATION

Figure 1a displays a schematic of the longitudinal cross-section of a microfluidic channel where two parallel, planar gold

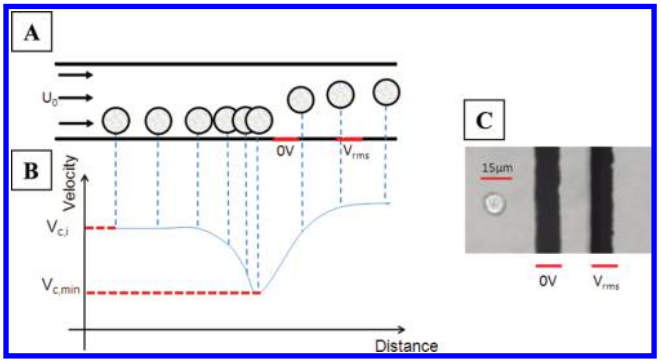

Figure 1. A. Schematic of the microfluidic flow cell with embedded planar electrodes. B. Corresponding cell velocity as a function of traveling time. C. Bright field snapshot of a live T-cell approaching the electrodes.

electrodes are embedded on a glass substrate. Here the goal is to ensure that each cell encounters the same electric gradient perpendicular to the flow path and that the drag force overcomes the dielectrophoretic force. This forces cells to transit through the DEP barrier. As a consequence, close to the high electric field region, cells will slow down before being lifted up and pass over electrodes. This deceleration pattern is graphically represented in Figure 1b. Figure 1c is a bright field top view of a live cell approaching the patterned electrodes. The voltage is kept constant at 3.5 V_{rms}.

THEORY OF OPERATION

The balance between the DEP and drag forces strongly depends on the characteristic lengths of the system. Importantly, the mass density of Jurkat cells higher than water[15] combined with the restriction in channel height ensures the vast majority of cells will be immersed in the high electric field region. Assuming that cells flow at constant velocity (no drag) toward electrodes, the DEP force ($\vec{F}_{DEP}$) will exert a backward component close to the electrode edge that causes deceleration. This is combined with electro-hydrodynamic (EHD) flows which are assumed to form a constant flow field.[16] At this point, the drag force $\vec{F}_{Drag}$ increases and the cell forced to overcome the DEP/EHD barrier. Assuming a quasi-trapping regime, the DEP, EHD, and drag forces are approximately equal near the electrodes where velocity is at a minimum, that is,

$$|\vec{F}_{Drag}| \approx |\vec{F}_{DEP}| + |\vec{F}_{EHD}| \quad (1)$$

EHD flows are created by local temperature rise close to the electrodes giving rise to both conductivity and permittivity gradients. In our system, maximum temperature rise can be estimated to less than 10 °C at 3.5 Vrms.[10,17] EHD flows are supposed to be steady and the corresponding force proportional to the volume of the cells. The latter therefore scales with the cube of the cell radius as does DEP. Combination of eq 1 with the classical time-averaged DEP force expression yields

$$k\frac{V_{c,i} - V_{c,min}}{R^2} \approx \frac{\varepsilon_m \,\mathrm{Re(CM)}}{3\eta}\nabla|\vec{E}|^2 + C_{EHD} \quad (2)$$

Here $V_{c,i}$ and $V_{c,min}$ are the incoming and minimum cell velocity, respectively, k is a nondimensional correction factor for the wall effect,[18] C_{EHD} is a constant factoring in EHD contributions, and R is the radius of the cell in micrometers. CM is the Clausius-Mossotti factor, ε_m is the absolute permittivity of the medium, η is the dynamic viscosity of the medium, and $\vec{E}$ is the electric field.

From eq 2, a slowing down factor S can be defined, normalizing for incoming cell velocity:

$$S = \frac{V_{c,i} - V_{c,min}}{V_{c,i}}\frac{1}{R^2} \quad (3)$$

Using such a definition, the slowing down factor will be 0 for cells with no measurable change in velocity and approximately $1/R^2$ for cells strongly decelerated. This factor has to be finally linearly corrected to compensate for the fact the residence time in the high electric field region decreases with increasing flow velocity. If the electric field is kept constant, the slowing down factor reflects the response of the cell. After deceleration, cells are repelled vertically and accelerate toward a faster streamline as found in DEP-FFF. However, the exiting velocity in a shallow channel is a complex correlation between incoming the cell height, local electrohydrodynamic flow (driven by the temperature and permittivity gradient over the electrodes), cell rotation, and surface−cell interactions. Indeed, the key to performing a quantitative analysis is to devise a system where any cell starts at an identical point of origin. This way, any differences in DEP response can translate into quantifiable differences in flow patterns.

FREQUENCY RESPONSE OF CELLS IN PHYSIOLOGICAL BUFFERS

As cell response varies significantly over the typical DEP frequency range [100 kHz−100 MHz], an understanding of the different frequency regimes allows for interrogation of distinct dielectric properties. Assuming Maxwell−Wagner−Sillars inter-

dx.doi.org/10.1021/ac2022103 | Anal. Chem. 2012, 84, 1849−1853

facial polarization, the transition between conductivity dominated behavior and the dielectric permittivity regime is found in excess of 250 MHz for cells in high conductivity buffers. Above this value, the cell response is dominated by dielectric permittivity differences. Because the cell cytoplasm has a dielectric permittivity very close to that of water, the response is close to zero above this transition frequency.

In the effective single shell model, the frequency spectrum of cells contains an intermediate region where the voltage drops almost entirely across the cell membrane. In high conductivity buffers (>1 S/m), this region is located between 1 and 100 MHz, with a characteristic plateau being strongly dependent on cytoplasm conductivity. An analytical expression can be derived from the theory described in ref 19 and applied to the case of high conductivity buffers (see Supporting Information), that is,

$$\mathrm{Re(CM)} \approx \frac{\sigma_c - \sigma_m}{\sigma_c + 2\sigma_m} \tag{4}$$

Here σ_c is the electrical conductivity of the cytoplasm and σ_m is the electrical conductivity of the medium. This dependence in conductivity of the cytoplasm is illustrated in Figure 2a. At low frequencies ($\ll$1 MHz), the membrane conductivity plays an important role in the overall cell response. Live cells with preserved membrane integrity typically have a very low conductivity (10^{-7} S/m) and a CM factor close to the minimum value of −0.5. Conversely, heat-treated cells exhibit a membrane conductivity increase by several orders of magnitude due to the formation of irreversible pores.[20] A change in membrane capacitance is also expected due to morphological changes that occur above the denaturation temperature of proteins. As mentioned in prior studies, the induced change in membrane capacitance strongly depends on the method used to kill cells and is therefore difficult to predict.[21]

If one assumes that the conductivity of the cell cytoplasm is less than or of the same order of magnitude as that of the medium, the low frequency response can be approximated (see Supporting Information) by

$$\mathrm{Re(CM)} \approx -\frac{{\sigma_m}^2}{2{\sigma_m}^2 + c\sigma_m\sigma_{mem}},$$
$$c = \frac{9R^3}{t(3R^2 - 3Rt + t^2)} - 4 \tag{5}$$

Here σ_{mem} is the conductivity of the membrane and t *is* the thickness of the lipid bilayer (7 nm). The significance of membrane conductivity variations in dead cells is illustrated in Figure 2b.

Membrane capacitance influences the transition frequency between low and intermediate responses. However, a simulated change from 10 mF/m^2 to 15 mF/m^2 will trigger a change in the cell response lower than 10% for all frequencies. Simulation plots for membrane capacitance change are given in the Supporting Information.

This theoretical analysis shows that significant differences in DEP response for live and heat-treated mammalian cells can be seen through independent levels within distinct frequency bands.[7]

RESULTS

By testing a range of incoming velocities, the slowing down factor was calculated and plotted for frequencies of 1 and 40 MHz (Figure 3). Details of the calculation of the slowing down

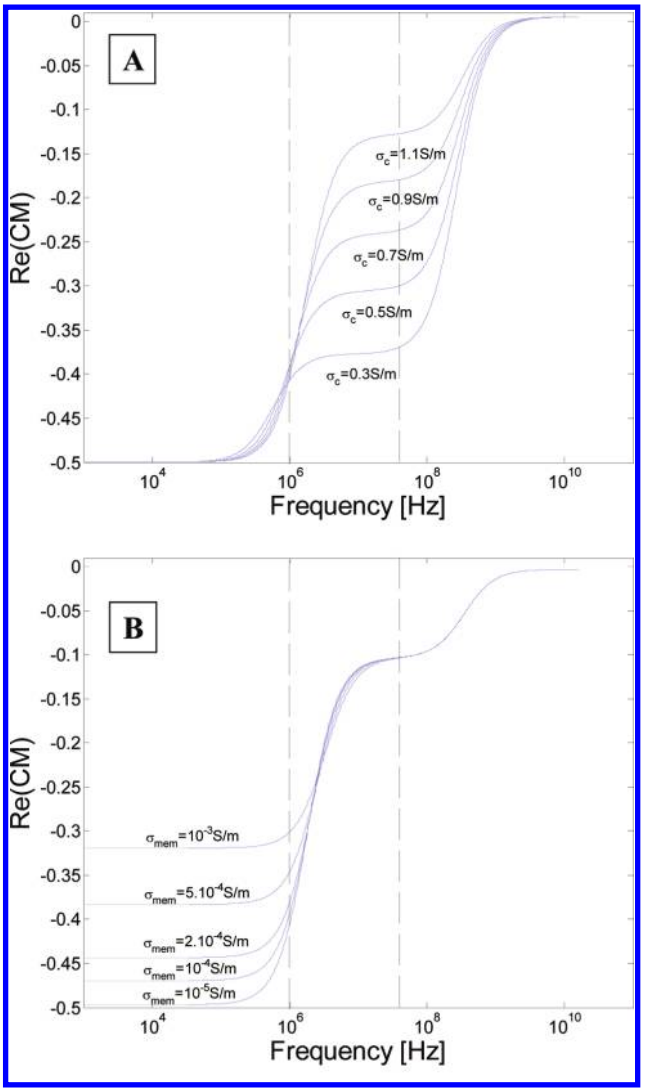

Figure 2. Theoretical frequency response of cells in a high conductivity buffer based on the effective single-shell model. Vertical dashed lines indicate 1 MHz and 40 MHz. A. The cell cytoplasm conductivity changes from 0.3 S/m to 1.1 S/m using a set membrane conductivity of 10^{-7} S/m (case of a live cell) and membrane capacitance of 13 mF/m^2. B. The cell membrane conductivity changes from 10^{-5}S/m to 10^{-3} S/m for a set cytoplasm conductivity of 1.2S/m (case of a dead cell) and membrane capacitance of 13 mF/m^2.

factor are included in the Supporting Information. Given the high electric field gradients (in excess of 10^5 V/m), the occurrence of AC electro-osmosis prevents access to frequencies much lower than 1 MHz.

The observed dispersion of data points can be accounted for by differences in incoming depth, variability in cell morphology, and intrinsic biological variability, with each cell having a unique set of dielectric parameters. Strategies to reduce this dispersion include decreasing the channel height or parallelization of the electrode pattern. For velocities greater than 200 μm/s, the time resolution needed to monitor slowing down events has to be increased.

The data from the scatter histograms in Figure 3 are summarized in Table 1. The distributions were fitted to a Gaussian model having the functional form $Ae^{-[(S-\mu)^2/(2\sigma^2)]}$.

The ellipses plotted in Figure 3 represent a confidence limit of one standard deviation. The area overlap between the two

dx.doi.org/10.1021/ac2022103 | *Anal. Chem.* 2012, 84, 1849−1853

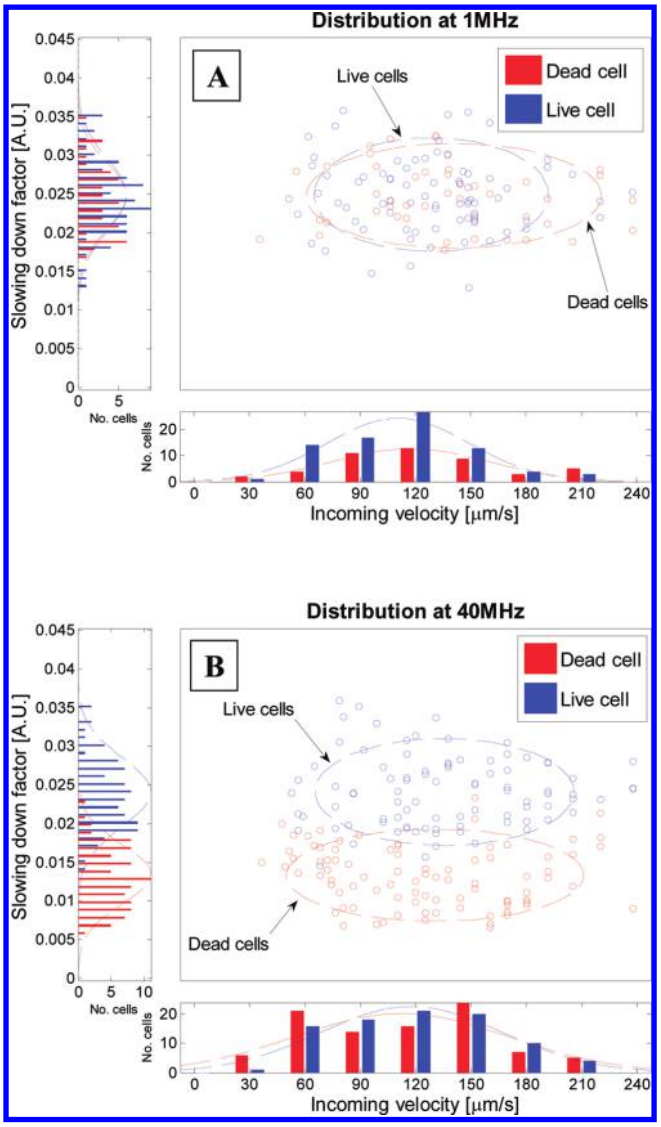

Figure 3. Slowing down factor versus incoming velocity at 1 MHz (A) and 40 MHz (B) exhibit the presence of two distinct populations. The probability ellipses for both distributions correspond to 1σ.

Table 1. Number of Cells Screened for Each Frequency and Fitting Parameters with Mean μ and Standard Deviation σ for the Gaussian Fits of Histograms of Slowing down Factors at 1 MHz and 40 MHz

	live cells		dead cells	
	1 MHz	40 MHz	1 MHz	40 MHz
number of cells tested	79	90	48	95
A	7.14	7.94	4.14	8.93
μ [a.u.]	0.024	0.023	0.024	0.013
σ [a.u.]	6×10^{-3}	6×10^{-3}	7×10^{-3}	6×10^{-3}

ellipses is 77% at 1 MHz and 5% at 40 MHz. For two standard deviations, the overlap of the ellipses becomes 79% at 1 MHz and 25% at 40 MHz.

Using simulation plots, mean slowing down factors were used to set up a qualitative analysis of frequency responses. The consistency between the response of live cells at both 1 MHz and 40 MHz indicates the cell cytoplasm had a conductivity much lower than the buffer. This is in broad agreement with previous studies suggesting the presence of ion flow barriers within live cells.[22,23]

The large difference in response seen at 40 MHz between live and dead cells is primarily accounted for by cytoplasmic conductivity differences. This confirms that the increased permeability during the heat treatment led to an increased cytoplasm conductivity. As the response was found only halved compared to live cells, this also suggests that organelles within the cytoplasm do behave as resistive elements even though the intracellular ionic strength would be of similar value to that of the buffer.

Overall, the analysis of the frequency bands gives insight into how to exploit the dielectric properties of live and heat-treated cells and forms the basis for future separation works.

CONCLUSION

A scheme for sensing cell response within a nonuniform field in a highly conductive buffer has been devised and successfully applied to the identification of live and dead Jurkat T-cells. This functional scheme exploits both geometrical and electrical confinement effects. Operation at a frequency of 40 MHz was found to achieve efficient cell identification based on dielectric properties that vary due to a change in membrane permeability. This technique can be readily adapted to the screening of apoptotic cells experiencing changes in their DEP response spectrum.[24,25] Importantly, the architecture is adaptable and is likely to find application in other areas of high-throughput detection and counting of cells in physiological buffers. The complete automation of the proposed architecture to a sorting system could be achieved by coupling the particle image velocimetry method to an active valve system. Parallelization of the electrode pattern along the fluidic microchannel could also provide multiple screening steps that would further reduce the error contributions brought about by hydrodynamics.

Selective trapping of live cells can also be achieved when operating at lower flow rates. It will be especially useful to quickly identify mixtures of cells having different dielectric properties without introducing changes to their suspending environment.

ASSOCIATED CONTENT

Supporting Information

Approximations of cell responses at intermediate and low frequencies in a high conductivity buffer, influence of cell membrane capacitance on the dielectric response, and calculation of the slowing down factor. This material is available free of charge via the Internet at http://pubs.acs.org.

AUTHOR INFORMATION

Corresponding Author

*E-mail: joshua.edel@imperial.ac.uk.

ACKNOWLEDGMENTS

This work was supported in part by the EPSRC-funded doctoral training centre in chemical biology at the Institute of Chemical Biology, Imperial College London, and an RCUK basic technology and platform grant, along with an ERC Starting grant.

REFERENCES

(1) Markx, G. H.; Talary, M. S.; Pethig, R. *J. Biotechnol.* **1994**, 32 (1), 29–37.

(2) Fiedler, S.; Shirley, S. G.; Schnelle, T.; Fuhr, G. *Anal. Chem.* **1998**, *70* (9), 1909−1915.
(3) Muller, T.; Pfennig, A.; Klein, P.; Gradl, G.; Jager, M.; Schnelle, T. *IEEE Eng. Med. Biol. Magazine* **2003**, *22* (6), 51−61.
(4) Huang, Y.; Holzel, R.; Pethig , R.; Wang, X.-B. *Phys. Med. Biol.* **1992**, *37* (7), 1499−1517.
(5) Pethig, R. *Biomicrofluidics* **2010**, *4* (2), 35.
(6) Lapizco-Encinas, B. H.; Simmons, B. A.; Cummings, E. B.; Fintschenko, Y. *Anal. Chem.* **2004**, *76* (6), 1571−1579.
(7) Huang, Y.; Joo, S.; Duhon, M.; Heller, M.; Wallace, B.; Xu, X. *Anal. Chem.* **2002**, *74* (14), 3362−3371.
(8) Mernier, G.; Piacentini, N.; Braschler, T.; Demierre, N.; Renaud, P. *Lab Chip* **2010**, *10* (16), 2077−2082.
(9) Puttaswamy, S. V.; Sivashankar, S.; Chen, R.-J.; Chin, C.-K.; Chang, H. Y.; Liu, C. H. *Biotechnol. J.* **2010**, *5* (10), 1005−1015.
(10) Gielen, F.; Pereira, F.; deMello, A. J.; Edel, J. B. *Anal. Chem.* **2010**, *82* (17), 7509−7514.
(11) Watarai, H.; Sakamoto, T.; Tsukahara, S. *Chem. Lett.* **1998**, No. 3, 279−280.
(12) Kaler, K.; Jones, T. B. *Biophys. J.* **1990**, *57* (2), 173−182.
(13) Wang, X. B.; Vykoukal, J.; Becker, F. F.; Gascoyne, P. R. C. *Biophys. J.* **1998**, *74* (5), 2689−2701.
(14) Gielen, F.; deMello, A. J.; Cass, T.; Edel, J. B. *J. Phys. Chem. B* **2009**, *113* (5), 1493−1500.
(15) Jaggi, R. D.; Sandoz, R.; Effenhauser, C. S. *Microfluid. Nanofluid.* **2007**, *3* (1), 47−53.
(16) Morgan, H.; Green, N. *AC Electrokinetics: colloids and nanoparticles*; Research Studies Press: Baldock, 2003.
(17) Grom, F.; Kentsch, J.; Müller, T.; Schnelle, T.; Stelzle, M. *Electrophoresis* **2006**, *27* (7), 1386−1393.
(18) Li, H. B.; Zheng, Y.; Akin, D.; Bashir, R. *J. Microelectromech. Syst.* **2005**, *14* (1), 103−112.
(19) Jones, T. B. *Electromechanics of particles*; Cambridge University Press: 1995.
(20) Alder, G. M.; Austen, B. M.; Bashford, C. L.; Mehlert, A.; Pasternak, C. A. *Biosci. Rep.* **1990**, *10* (6), 509−518.
(21) Pethig, R.; Talary, M. S. *IET Nanobiotechnol.* **2007**, *1* (1), 2−9.
(22) Huang, Y.; Wang, X. B.; Hölzel, R.; Becker, F. F.; Gascoyne, P. R. *Phys. Med. Biol.* **1995**, *40* (11), 1789−1806.
(23) Asami, K.; Takahashi, Y.; Takashima, S. *Biochim. Biophys. Acta* **1989**, *1010* (1), 49−55.
(24) Wlodkowic, D.; Khoshmanesh, K.; Sharpe, J. C.; Darzynkiewicz, Z.; Cooper, J. M. *Anal. Chem.* **2011**, *83* (17), 6439−6446.
(25) Khoshmanesh, K.; Akagi, J.; Nahavandi, S.; Skommer, J.; Baratchi, S.; Cooper, J. M.; Kalantar-Zadeh, K.; Williams, D. E.; Wlodkowic, E. *Anal. Chem.* **2011**, *83* (6), 2133−2144.